S. Deng, G. R. MacCartney, Jr., and T. S. Rappaport, "Indoor and Outdoor 5G Diffraction Measurements and Models at 10, 20 , and 26 Ghz," in *2016 IEEE Global Communications Conference (GLOBECOM)*, Dec. 2016.

Indoor and Outdoor 5G Diffraction Measurements and Models at 10, 20, and 26 GHz

Sijia Deng, *Student Member, IEEE,*
George R. MacCartney, Jr., *Student Member, IEEE,*
Theodore S. Rappaport, *Fellow, IEEE*

***Abstract*—This paper presents diffraction measurements, analysis, and signal strength prediction models around objects such as corners, pillars, and irregular objects, at 10, 20, and 26 GHz. The diffraction measurements were conducted indoors and outdoors by using a continuous wave (CW) channel sounder with three pairs of identical directional horn antennas at the transmitter and receiver. The measurement results are compared with theoretical predictions based on the Knife Edge Diffraction (KED) in order to determine how well the theoretical model compares to real-world measurements. The KED model is shown to work well for indoor environments, and an empirical linear model with a fixed reference point is also presented and provides a better fit to the measured data around rounded corners in the outdoor environment. Diffraction loss is shown to increase with frequency in outdoor scenarios, but less so inside buildings due to reflection and transmission between walls. The model validation and new models will be useful for designing and calibrating ray-tracers and other wireless network simulators by simulating potential channel loss from diffraction around objects and understanding the impact of diffraction at centimeter-wave and millimeter-wave frequencies in indoor and outdoor environments.**

***Index Terms*—Millimeter-wave, centimeter-wave, diffraction, 5G, propagation, path loss, prediction model, continuous wave.**

I. Introduction

The growth of mobile communications and advances in wireless technology are leading the world towards a fully connected society. In order to support increasing capacity demand, future wireless systems are expected to operate at higher centimeter-wave (cmWave) and millimeter-wave (mmWave) frequencies, harmoniously with the saturated sub-6 GHz frequencies of current cellular systems [1]. The performance of a radio communications system is strongly determined by the propagation mechanisms that give rise to the received signals [2]. In many situations, mechanisms such as attenuation due to transmission through obstacles, depolarization, specular reflection, diffraction, or scattering will significantly improve or limit the quality of the radio link.

The development of cmWave and mmWave communication systems will require accurate models of radio channel properties [3]. While the feasibility of signal transmission in the mmWave frequency range has been successfully demonstrated [4], [5], the reliable prediction of coverage and system performance based on computer simulation and design tools, such as ray tracers, requires accurate knowledge of reflection, scattering, and diffraction effects [6], [7]. These mechanisms are important to understand at cmWave and mmWave frequencies because of the small transmission wavelength and also the need to overcome the additional free space path loss in the first meter of propagation when compared with lower UHF/microwave frequencies [8], [9].

Over the past few decades, diffraction has been thoroughly studied at conventional bands below 6 GHz, yet it has not been sufficiently explored in the cmWave and mmWave bands. Some of the few existing measurements and studies were conducted at 10 GHz [10], 28 GHz [11], and 60 GHz [12], [13]. Jacob *et al.* presented extensive measurements and ray tracing investigations on diffraction for 60 GHz and 300 GHz indoor channels [12]. Results showed that diffraction at edges or wedges can be neglected regardless of the frequency for line-of-sight (LOS) cases, and in the non-LOS (NLOS) cases, measured propagation loss matched well with the Uniform Theory of Diffraction (UTD) model [12].

Tervo *et al.* demonstrated a good match between measurements and the KED and UTD models for diffraction around corners at 10 GHz in the shadow region, but found a poor fit to measurement data close to the shadow boundary and in the illuminated or lit region [10]. Lu *et al.* showed that diffraction measurements at 60 GHz were predicted well by the absorbing screen diffraction model with standard deviations of error less than 2.6 dB. [13]. Tenerelli *et al.* conducted a building corner diffraction measurement campaign at 28 GHz and presented a simple linear model to predict building corner diffraction

This material is based upon work supported by the NYU WIRELESS Industrial Affiliates Program, Nokia Solution and Networks, and three National Science Foundation (NSF) Research Grants: 1320472, 1302336, and 1555332, and the GAANN Fellowship Program. The authors would like to thank JP Ryan, Rieko Tsuji, and Shu Sun for the assistance with measurements. S. Deng (email: sijia@nyu.edu), G. R. MacCartney, Jr. (email: gmac@nyu.edu), and T. S. Rappaport (email: tsr@nyu.edu), are with the NYU WIRELESS Research Center, NYU Tandon School of Engineering, 9th Floor, 2 MetroTech Center, Brooklyn, NY 11201.

loss, and showed that diffraction loss grows logarithmically for small diffraction angles and linearly for large diffraction angles [11]. This paper aims to compare real world diffraction measurements with traditional theoretical models from 10 to 26 GHz, and presents new empirically-based diffraction models for wireless channel prediction.

II. Measurement Environment and Procedures

Diffraction measurements were conducted in both indoor and outdoor environments. Indoor diffraction measurements were performed at two 90° right-angle corners made of drywall and wood, and at the corner edge of a semi-transparent plastic board with a thickness of 2 cm as shown in Fig. 1. Outdoor diffraction measurements were performed at a 90° right-angle corner made of marble and a rounded corner stone pillar, as shown Fig. 2.

Measurements were performed by transmitting continuous wave (CW) signals at 10, 20, and 26 GHz for vertical-to-vertical (V-V) antenna polarization configurations with the TX and RX antennas set at heights of 1.4 m above the ground. The antenna gains and half-power-beamwidths (HPBW) were 20 dBi and 17°, respectively, for measurements at 10 and 20 GHz, and 24.5 dBi and 10.9°, respectively, for measurements at 26 GHz. The TX antenna was located on one side of a corner, and the RX antenna located on the other side of the corner was mounted on a rotating gimbal, which translated along a linear track. The distance from the TX antenna to the edge of the diffracted corner was always in the far field of the TX antennas, at a constant 2 m (d_1), and the distance from the edge of the corner to the RX antenna (also in the far field) was a constant 1 m (d_2) as shown in Fig. 3 (for the 26 GHz antennas, the far field distance is 1.1 m, a little bit larger than d_2). The TX antenna was adjusted to point to the edge of the corner for two or three fixed incident angles (β), approximately from 10° to 35°. The RX antenna translated along the linear track in step increments of 0.875 cm, which corresponds to approximately 0.5° increments of the diffraction angle (α). The RX antenna was adjusted to point to the edge of the corner at each track increment, with the RX power level measured by an Agilent E4407B spectrum analyzer. For each track location, the 35.5 cm long linear track was used to measure a 20° swath of diffraction angles in the horizontal plane (parallel to the ground). Five consecutive RX linear track locations were used to simulate a contiguous arc around the corner to measure a 100° swath of total diffraction angles, which enabled the RX antenna to move from the deep shadow region to the lit region.

A free space calibration was performed at each measured frequency at a TX-RX separation distance of 3 m (d_1+d_2 = 3 m). The relative diffraction loss was obtained by computing the difference between the calibration received power and the measured power level at each diffraction angle measurement (the antenna gains were removed as part of calibration).

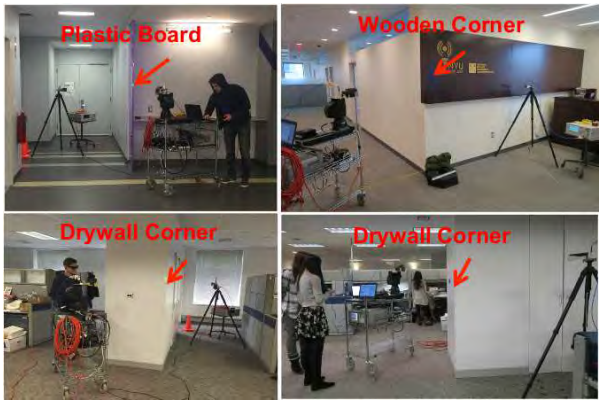

Fig. 1: Indoor diffraction measurements in NYU WIRELESS. Test locations include: a drywall corner with a straight (90°) edge, a semi-transparent plastic board with a relatively straight edge, and wood corner with a straight edge.

Fig. 2: TX and RX locations for outdoor diffraction measurements on the NYU campus. The test locations include a stone pillar with rounded (cylindrical) edges and a marble corner with a straight (90°) edge.

III. Theoretical Diffraction Models and Analysis

A. Knife Edge Diffraction (KED) Model

The knife edge diffraction model is commonly used in ray tracing simulations due to its simplicity and accuracy for diffraction loss prediction for many geometries [14]. The knife-edge effect can be explained by Huygen's principle,

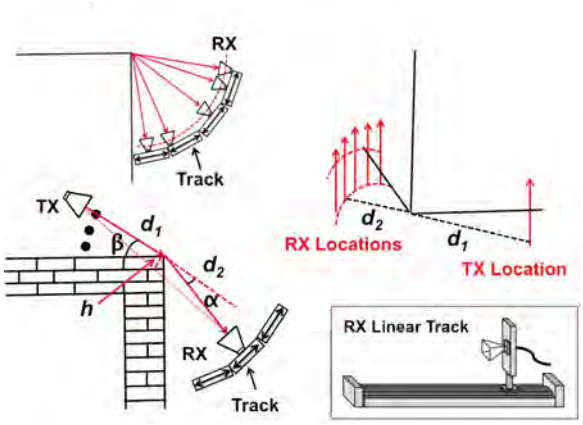

Fig. 3: Schematic of the corner diffraction geometry. The TX antenna was located on one side of the corner, while the RX antenna moved along a simulated arc on the other side of the corner. Diffraction angle (α) is defined as the angle between the direction of incident beam and any resulting diffracted beam.

which states that a well-defined obstruction acts as a secondary source to an electromagnetic wave, such that all points on a wavefront can be considered as point sources that produce secondary wavelets, and these wavelets combine to create a new wavefront in the direction of propagation [2]. The new wavefront thus propagates into the geometric shadow area of the obstacle, resulting in the diffraction phenomenon.

Diffraction loss over complex and irregular obstruction can be difficult to calculate; here we focused on simple obstructions that can provide an acceptable prediction on the magnitude of diffraction loss. Single objects, such as a corner can be considered as a simple diffracting knife edge.

The electric field strength E_d [V/m] at the RX is a vector sum of the fields of all secondary Huygen's sources in the plane of the knife edge, which is given by:

$$\frac{E_d}{E_0} = F(\nu) = \frac{1+j}{2}\int_v^\infty e^{-j(\pi/2)t^2}dt \tag{1}$$

E_0 [V/m] is the free space field strength and $F(\nu)$ is the complex Fresnel integral, where the Fresnel diffraction parameter ν can be written as [2]:

$$\nu = h\sqrt{\frac{2(d_1+d_2)}{\lambda d_1 d_2}} = \alpha\sqrt{\frac{2d_1d_2}{\lambda(d_1+d_2)}} \tag{2}$$

where λ is the wavelength, h is the effective height (or width) of the obstructing screen with infinite width (or height) placed between the TX and RX at the distances d_1 and d_2, respectively, under the conditions that d_1, $d_2 >> h$, and d_1, $d_2 >> \lambda$. These conditions were met for 10, 20 and 26 GHz measurements in both the indoor and outdoor environments, as shown in Fig. 3.

The diffraction gain in dB due to the presence of a knife edge, as compared to that observed in free space is calculated as:

$$G(\nu)[\text{dB}] = -P(\nu) = 20\log|F(\nu)| \tag{3}$$

where $G(\nu)$ is the gain of the diffracted signal and $P(\nu)$ is the loss of the diffracted signal (as compared to free space) for a given value of ν. This model is simple to implement and does not account for polarization effects nor the shape of the obstacles.

B. Diffraction From A Convex Surface

The KED model is one of the most commonly used methods of prediction but can only be used for sharp knife edges, and does not account for the radius of curvature of an obstacle. Many natural terrain features and building features exhibit curved surfaces, indicating that the radius of curvature should be accounted for.

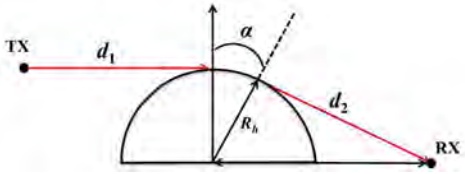

Fig. 4: Diffraction by a circular cylinder. α is the diffraction angle and R_h is the radius of the circle.

A creeping wave is the wave that is diffracted around the surface of a rounded obstacle such as a circular cylinder (see Fig. 4). The asymptotic representation for the creeping ray field [15] at the RX antenna behind the cylinder for an incident plane wave is proportional to:

$$E \sim E_i e^{-jk\alpha R_h}\frac{e^{-jkd_2}}{\sqrt{kd_2}}\sum_{p=1}^{\infty} D_p R_h \cdot \exp(-\psi_p \alpha) \tag{4}$$

where E_i is the incident field at the TX, d_2 is the distance from the launch point to the RX antenna, k is the wave number, and α is the diffraction angle. D_p is the excitation coefficient and ψ_p is the attenuation constant, which are functions of the cylinder radius and carrier frequency:

$$D_p, \psi_p \sim \left(\frac{kP_h}{2}\right)^{\frac{1}{3}} \tag{5}$$

The mathematical derivation of the asymptotic representation for the creeping ray can be found in [16]. A reasonable approximation for (4) on a flat surface can be obtained by keeping only the $p = 1$ term in (4). The representation of the creeping ray field is proportional to:

$$E \sim D_p R_h \cdot \exp(-\psi_p \alpha) \tag{6}$$

The diffraction gain/loss in dB due to the presence of an obstacle, as compared to the free space signal, can then be calculated as

$$\begin{aligned} G(\alpha)[\text{dB}] &= -P(\alpha) = 20\log_{10} E \\ &= -A(R_h, f)\psi_p\alpha + C(R_h, f) \end{aligned} \tag{7}$$

where $A(R_h, f)$ and $C(R_h, f)$ are functions of the radius of the object and carrier frequency, which are computationally expensive [16]. According to [10], a linear model for (7) can estimate diffraction loss from a curved surface at a single frequency.

$$P(\alpha) = n \cdot \alpha + c \tag{8}$$

where n is the slope value of the linear model, calculated from measurement data using minimum mean square error (MMSE) estimation. c is the anchor point of the linear model, which is set to 6.03 dB, corresponding to the diffraction loss predicted by the KED model at the 0° diffraction angle.

C. Statistics Between Measurements And Prediction

The agreement between the measurement and theoretical predication can be evaluated in terms of two parameters: mean error (ME) and standard deviation (SD) [17]. The error (in dB) between the measurement and the theoretical prediction for each diffraction angle (α) is defined as,

$$\Delta(\alpha_i)[\text{dB}] = P_{meas}(\alpha_i) - P_{pred}(\alpha_i) \tag{9}$$

The ME is an indicator for the overall trend of the prediction and an ME value of zero indicates that the estimation matches well to the measurement, and is defined as:

$$\text{ME}[\text{dB}] = \frac{1}{N}\sum_{i=1}^{N}\Delta(\alpha_i) \tag{10}$$

where N is the total number of diffraction angles measured in the shadow region.

The SD is computed as,

$$\text{SD}[\text{dB}] = \left[\frac{1}{N-1}\sum_{i=1}^{N}(\Delta(\alpha_i) - \text{ME})^2\right]^{\frac{1}{2}} \tag{11}$$

where $N-1$ is used for sample standard deviation calculation [17].

IV. Measurement Results and Analysis

A. Indoor Measurement Results

1) Drywall Corner Measurements: Drywall is one of the most common materials in indoor environments. Fig. 5 shows the measured relative diffraction losses at 10, 20, and 26 GHz as a function of diffraction angle at a drywall corner. The relative losses were measured at three different TX incident angles for each frequency. In the shadow region (for diffraction angles greater than 0°), a relatively good agreement can be observed between the measurement data and the KED model prediction computed by equation (3). When the RX antenna moved from the lit region to the shadow region, the relative diffraction loss increased to approximately 25 dB at a diffraction angle of 20°. The main mechanisms in the lit region are direct transmission through free space and reflections in the environment, which are not predicted by the KED model. Similar results at 10 GHz were also observed in [10]. Due to the reflective indoor environment and the possibility of transmission through the objects, the diffraction loss showed slight dependence on frequency, as Figures 5 - 7 show less loss occurs at lower frequencies in general (note that the green points represent less relative loss at 10 GHz). The simple KED model provides a reasonable fit to the measured data in the shadow region and near the shadow boundary for the drywall material. Table I provides the ME and SD values for each material and frequency. The ME values are close to zero, indicating a good overall match between the KED model and the measured data. The high SD values (approximately 5-6 dB) of the model as shown in the Table I, and the oscillation patterns observed in Fig. 5 can be explained by the fact that in the shadow region, the measured diffraction signal is a combination of corner diffraction and penetration through the material (absorbing material was not used due to cost and difficulty in ensuring that even with absorbing material, the only received energy was from diffraction). System engineers should take into account the high SD values and maximum diffraction loss in network simulation and design.

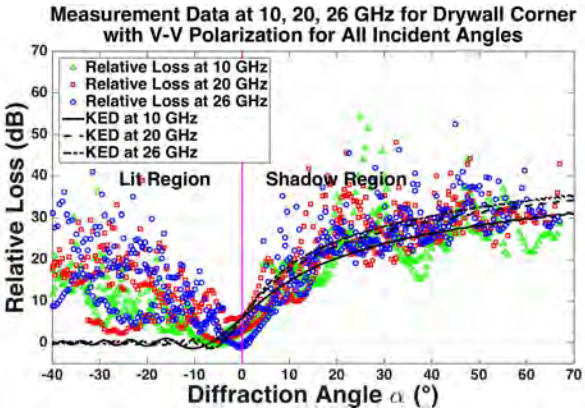

Fig. 5: Indoor drywall corner diffraction measurement results compared to the KED model at 10, 20, and 26 GHz.

2) Wooden Corner: Fig. 6 shows the indoor wooden corner measurement results for the set-up in Fig. 1, (note that the top part of the measured wooden corner is a wooden decoration with smooth surface, and the bottom part of the corner is

typical drywall in Fig. 1) compared to the KED prediction at 10, 20, and 26 GHz. According to the negative ME values in Table I, the KED model, in general, overestimates the observed diffraction loss by 3.32 dB, 3.88 dB and 1.54 dB at 10, 20, and 26 GHz, respectively, in the shadow region and near the shadow boundary. The measured diffraction loss increases to approximately 30 dB at a diffraction angle of 30°. The results between the drywall corner and wooden corner are comparable, indicating that frequency dependence on similar building materials is small for diffraction in the indoor environment. The high SD values (approximately 6 dB) and the oscillation patterns are probably due to penetration through the measured material and the reflective environment.

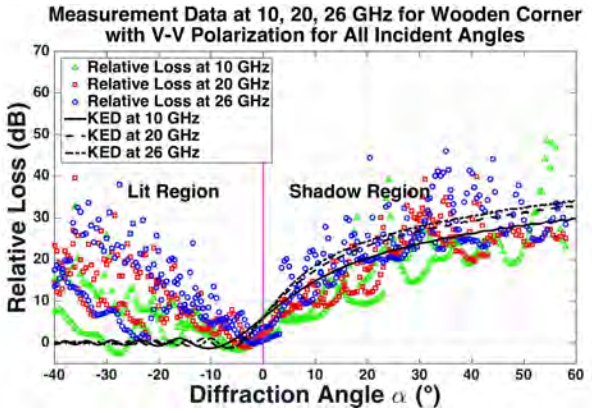

Fig. 6: Indoor wooden corner diffraction measurement results compared to the KED model at 10, 20, and 26 GHz.

3) Plastic Board: Fig. 7 shows the indoor plastic board measurement results compared to the KED prediction at 10, 20, and 26 GHz. For the shadow region near the shadow boundary (diffraction angle from 0° to 30°), the KED model overestimates the measured relative diffraction loss at small diffraction angles, but in the deep shadow region, the KED model slightly underestimates the measured relative diffraction loss, likely due to penetration through the semitransparent plastic board. According to the negative ME values in Table I, the KED model slightly overestimates the measurement results by 3.72 dB, 3.18 dB and 4.15 dB at 10, 20, and 26 GHz, respectively, in the shadow region and near the shadow boundary (not a substantial difference to the theory). As observed in all indoor scenarios, there is only slight frequency dependence, likely due to the reflective indoor environment and transmission through the diffraction object.

B. Outdoor Measurement Results

1) Stone Pillar: Fig. 8 shows the outdoor stone pillar (e.g. cylindrical object) measurement results at 10 GHz compared to the KED model and linear model. From the plot, the linear model using MMSE estimation computed by (8) provides a

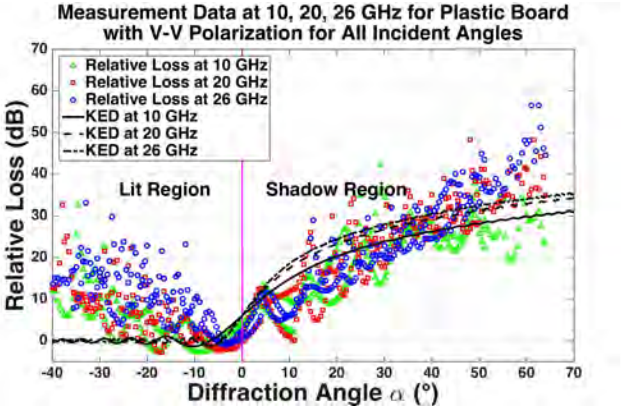

Fig. 7: Indoor plastic board diffraction measurement results compared to the KED model at 10, 20, and 26 GHz.

TABLE I: Mean error and standard deviation between the measurement data and KED model prediction (by using equation (3)) for each frequency and material in the indoor environment.

Material	Frequency (GHz)	ME (dB)	SD (dB)
Drywall	10	**0.49**	**5.79**
	20	**0.11**	**5.43**
	26	**-1.34**	**5.06**
Wood	10	**-3.32**	**5.77**
	20	**-3.88**	**4.36**
	26	**-1.54**	**5.21**
Plastic	10	**-3.72**	**4.56**
	20	**-3.18**	**5.24**
	26	**-4.15**	**7.14**

better fit to the measured relative diffraction loss in the shadow region than the KED model. The anchor point of the linear model is 6.03 dB, which is the corresponding diffraction loss predicted by KED at the 0° diffraction angle. The slope of the linear model is 0.75 at 10 GHz, and is a much better fit to the measured data, as the KED model underestimates diffraction loss for diffraction angles greater than 20°.

Fig. 9 shows the outdoor stone pillar measurement results compared to the linear model prediction at 10, 20, and 26 GHz. The relative loss for each frequency includes measured loss at two TX incident angles, and is plotted as a function of diffraction angle. In the shadow region, a good agreement is observed between the measured data with linear model prediction. The linear model slopes are 0.75, 0.88, and 0.96 for measurements at 10 GHz, 20 GHz, and 26 GHz, respectively. It is worth noting that the diffraction loss increases with frequency, resulting in increased slope values as frequency increases, for the linear model. The simple linear model provides a reasonable fit to the measured data with lower standard deviation compared with the KED model in

the shadow region. Table III provides the ME, SD, and RMSE values for each material and frequency. The ME values are close to zero, as well as small SD values, indicating a good overall match between the linear model and the measured data.

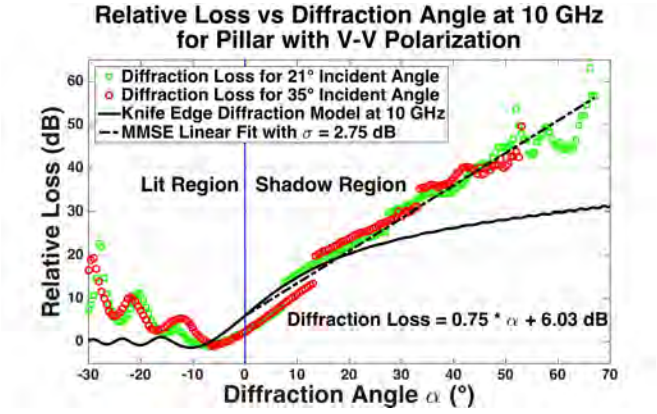

Fig. 8: Outdoor stone pillar diffraction measurement results compared to the KED and the empirical linear MMSE models at 10 GHz.

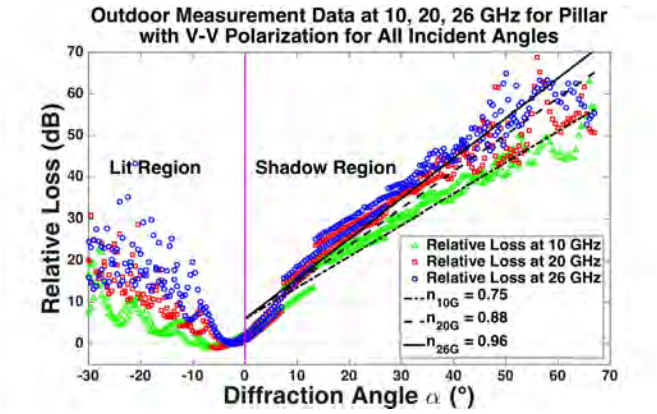

Fig. 9: Outdoor stone pillar diffraction measurement results compared to the empirical linear MMSE model at 10, 20, and 26 GHz.

2) Marble Corner: Fig. 10 shows the outdoor marble corner (with a straight edge) measurement results compared to the KED model and the linear MMSE model at 10 GHz. From the plot, the linear model provides a better fit to the measured relative diffraction loss in the shadow region, while the KED model underestimates diffraction for diffraction loss angles greater than 30°. The slope of the linear model is 0.62 at 10 GHz.

Fig. 11 shows the outdoor marble corner measurement results compared to the linear model prediction at 10, 20, and 26 GHz. In the shadow region, a good agreement is observed between the measured data and the linear MMSE model prediction (8). The slope values of the linear model are 0.62, 0.77, and 0.96 for measurements at 10 GHz, 20 GHz, and 26 GHz, respectively. Similar to observations made for the stone pillar, the diffraction loss increases at the marble corner with increasing frequency. Table II provides the slope values of the empirical linear MMSE model at 10, 20, and 26 GHz. Measurements conducted at the material with a rougher surface (stone) with a cylindrical shape usually resulted in a larger slope value than the material with a smoother surface (marble) with a straight edge. More measurements on other typical outdoor materials will be needed for a thorough comparison. The slope values of the linear model were observed to increase with frequency and with the roughness of the diffracted surface. Typical slope values calculated from the measurements ranged from 0.62 to 0.96 for both materials. The intention to use the MMSE method to derive the typical slope values instead of computing the theoretical slope value is to provide system engineers with a useful parameter while simplifying the computational process and cost. The ME values of the linear model for both the stone pillar and marble corner are close to zero for all frequencies, indicating a good overall match between the linear model and the measured data. Penetration through the marble corner is probably more prevalent than the stone pillar, resulting in higher SD values and more obvious oscillation patterns in the marble corner measurements.

TABLE II: Slope values of the linear MMSE model (using (8)) from the stone pillar and marble corner measurements at 10, 20, and 26 GHz.

Frequency (GHz)	Stone (n)	Marble (n)
10	**0.75**	**0.62**
20	**0.88**	**0.77**
26	**0.96**	**0.96**

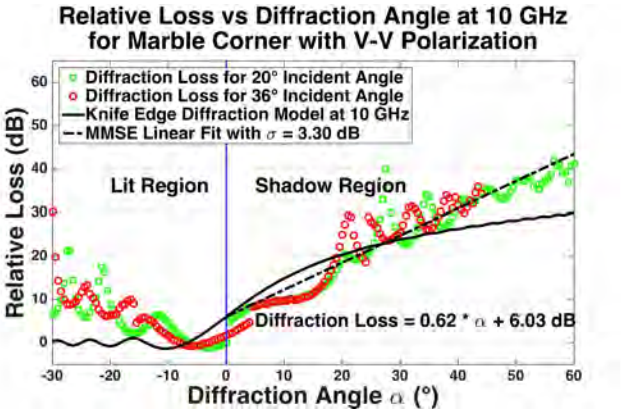

Fig. 10: Outdoor marble corner diffraction measurement results compared to the KED and the linear MMSE models at 10 GHz.

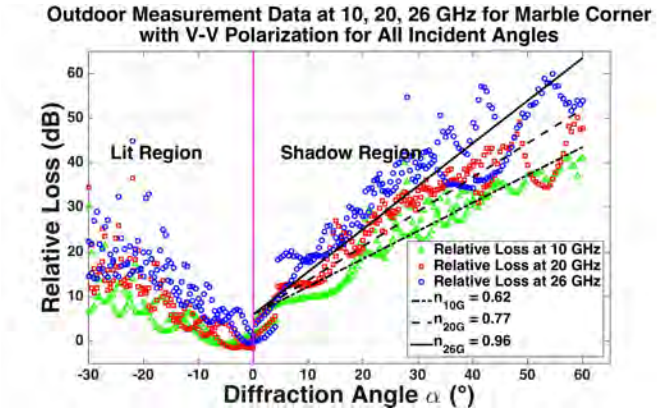

Fig. 11: Outdoor marble corner diffraction measurement results compared to the linear MMSE model at 10, 20, and 26 GHz.

TABLE III: Mean error and standard deviation between the measurement data and the linear MMSE model prediction (by using equation (8)) for each frequency and material in the outdoor environment.

Material	Frequency (GHz)	ME (dB)	SD (dB)
Pillar	10	**0.03**	**2.75**
	20	**0.45**	**4.31**
	26	**0.48**	**3.97**
Marble	10	**-0.34**	**3.30**
	20	**0.55**	**3.97**
	26	**1.05**	**5.41**

V. Conclusion

This paper presented indoor and outdoor diffraction measurements conducted for different materials at 10, 20, and 26 GHz. The indoor measurements around drywall corners showed a relatively good agreement between the measured relative diffraction loss and prediction by the KED model at all frequencies. For measurements conducted around the wooden corner and plastic board, the KED model only slightly overestimated the relative diffraction loss in the shadow region by 2-4 dB. Due to the reflective indoor environment and penetration through measured materials, the diffraction loss was observed to increase with increasing frequency, although there was variation in the data. The KED model can be used in ray tracing tools to calculate diffraction loss (considering approximately 5-6 dB standard deviation) in the indoor environment. The diffraction loss for an outdoor building corner with rounded edges can be better predicted by a simple linear model with a fixed anchor point rather than the KED model. The diffraction loss clearly increased with frequency for identical outdoor measurement locations. Typical slope values found in the measurements increased from 0.62 to 0.96, and these slope values may be used in ray tracing tools that incorporate the linear model. The simple KED model and linear MMSE model can be used in indoor and outdoor environments, respectively, to estimate propagation loss due to diffraction by building corners, for network simulations and ray-tracers, with good accuracy and short computation time. The results will allow wireless engineers to accurately model the propagation mechanism of diffraction for various materials at 10, 20, and 26 GHz when designing systems for cmWave and mmWave deployment.

References

[1] T. S. Rappaport, R. W. Heath, Jr., R. C. Daniels, and J. N. Murdock, *Millimeter Wave Wireless Communications*. Pearson/Prentice Hall, 2015.

[2] T. S. Rappaport, *Wireless Communications: Principles and Practice*, 2nd ed. Upper Saddle River, NJ: Prentice Hall, 2002.

[3] Z. Pi and F. Khan, "An introduction to millimeter-wave mobile broadband systems," *IEEE Communications Magazine*, vol. 49, no. 6, pp. 101–107, June 2011.

[4] T. S. Rappaport and et al., "Millimeter Wave Mobile Communications for 5G Cellular: It Will Work!" *IEEE Access*, vol. 1, pp. 335–349, 2013.

[5] G. R. MacCartney, Jr. and T. S. Rappaport, "73 GHz millimeter wave propagation measurements for outdoor urban mobile and backhaul communications in New York City," in *2014 IEEE International Conference on Communications (ICC)*, June 2014, pp. 4862–4867.

[6] G. Durgin, N. Patwari, and T. S. Rappaport, "An advanced 3d ray launching method for wireless propagation prediction," in *IEEE Vehicular Technology Conference*, vol. 2, May 1997, pp. 785–789.

[7] K. R. Schaubach, N. Davis, and T. S. Rappaport, "A ray tracing method for predicting path loss and delay spread in microcellular environments," in *IEEE Vehicular Technology Conference*, 1992, pp. 932–935.

[8] G. R. MacCartney, Jr., T. S. Rappaport, S. Sun, and S. Deng, "Indoor office wideband millimeter-wave propagation measurements and models at 28 GHz and 73 GHz for ultra-dense 5G wireless networks (invited)," *IEEE Access*, vol. 3, pp. 2388–2424, Oct. 2015.

[9] T. S. Rappaport *et al.*, "Wideband millimeter-wave propagation measurements and channel models for future wireless communication system design (invited paper)," *IEEE Transactions on Communications*, vol. 63, no. 9, pp. 3029–3056, Sept. 2015.

[10] N. Tervo and et al., "Diffraction measurements around a building corner at 10 GHz," in *2014 1st International Conference on 5G for Ubiquitous Connectivity (5GU)*, Nov. 2014, pp. 187–191.

[11] P. Tenerelli and C. Bostian, "Measurements of 28 GHz diffraction loss by building corners," in *The Ninth IEEE International Symposium on Personal, Indoor and Mobile Radio Communications*, vol. 3, Sep. 1998, pp. 1166–1169.

[12] M. Jacob and et al., "Diffraction in mm and sub-mm wave indoor propagation channels," *IEEE Transactions on Microwave Theory and Techniques*, vol. 60, no. 3, pp. 833–844, March 2012.

[13] J. Lu, P. Cabrol, D. Steinbach, and R. Pragada, "Measurement and characterization of various outdoor 60 GHz diffracted and scattered paths," in *IEEE Military Communications Conference (MILCOM)*, Nov. 2013, pp. 1238–1243.

[14] T. Russell, C. Bostian, and T. Rappaport, "A deterministic approach to predicting microwave diffraction by buildings for microcellular systems," *IEEE Transactions on Antennas and Propagation*, vol. 41, no. 12, pp. 1640–1649, Dec. 1993.

[15] L. Piazzi and H. L. Bertoni, "Effect of terrain on path loss in urban environments for wireless applications," *IEEE Transactions on Antennas and Propagation*, vol. 46, no. 8, pp. 1138–1147, Aug 1998.

[16] J. Keller, "Diffraction of a convex cylinder," *IRE Transactions on Antennas and Propagation*, vol. 4, no. 3, pp. 312–321, July 1956.

[17] T. Negishi and et al., "Measurements to validate the UTD triple diffraction coefficient," *IEEE Transactions on Antennas and Propagation*, vol. 62, no. 7, pp. 3723–3730, July 2014.